Journal of Molecular Catalysis A: Chemical 346 (2011) 79–86

Contents lists available at ScienceDirect

Journal of Molecular Catalysis A: Chemical

journal homepage: www.elsevier.com/locate/molcata

Catalytic performance of rare earth oxides in ketonization of acetic acid

Yasuhiro Yamada*, Masaki Segawa, Fumiya Sato, Takashi Kojima, Satoshi Sato*

Graduate School of Engineering, Chiba University, Yayoi, Inage, Chiba 263-8522, Japan

ARTICLE INFO

Article history:
Received 26 May 2011
Received in revised form 26 June 2011
Accepted 27 June 2011
Available online 2 July 2011

Keywords:
Ketonization
Acetic acid
Acetone
Rare earth oxides
Surface acetate species

ABSTRACT

A series of rare earth oxides were investigated as catalysts in the ketonization of acetic acid. High selectivity to acetone over 99% was obtained by reacting acetic acid over rare earth oxides such as La_2O_3, CeO_2, Pr_6O_{11}, and Nd_2O_3. Especially, Pr_6O_{11} showed the highest yield of 80% at 350 °C among the 14 rare earth oxides. The bulk structure of CeO_2 was stable during the ketonization, while the surface acetate species were observed over CeO_2 after ketonization. In contrast, the other active rare earth oxides such as La_2O_3, Pr_6O_{11}, and Nd_2O_3 were mainly basic oxides due to the formation of bulk oxyacetate such as MO(AcO), where M is La, Pr, and Nd and AcO indicates CH_3COO group, in the initial period of the reaction. In any case, the catalytic ketonization proceeds over the surface of the oxyacetates and CeO_2. Catalytic cycle of the ketonization is composed of two steps: the decomposition of surface $M_2O(AcO)_4$ to produce MO(AcO), acetone, and carbon dioxide and the regeneration of surface $M_2O(AcO)_4$ by reacting MO(AcO) and acetic acid to produce water.

1. Introduction

Since the mid-nineteenth century, the formation of ketone in the pyrolysis of metal salts of carboxylic acid has been known, which is introduced in a literature [1]. Synthesis of ketones from carboxylic acids in the vapor phase is called ketonization. Ketonization of carboxylic acid proceeds via the condensation reaction of two molecules of carboxylic acids to produce a ketone together with CO_2 and H_2O. The ketonization of carboxylic acid over catalysts such as Bi_2O_3 [2,3], CuO [2,3], Co_3O_4 [2,3], Cr_2O_3 [2–5], Al_2O_3 [2,3,6], PbO_2 [2,3], TiO_2 [2,3,7–9], ZrO_2 [2,3,8,10–12], CeO_2 [12–17], iron oxide [2,3,8,18–20], manganese oxide [2,3,12,13,16,21], V_2O_5 [8], MgO [22], Mg/Al hydrotalcites [23], and CeO_2-metal oxide [24,25] has been reported. However, mechanisms for the ketonization are still under debate.

Recently, Renz has reviewed mechanisms on the ketonization of carboxylic acid [26]. One of the proposed mechanisms involves an abstraction of alpha-hydrogen of carboxylic acid and forms ketene-like intermediate [17]. Another mechanism goes through an adsorbed carboxylate intermediate [3,24,26] which reacts with another carboxylate to produce ketone and CO_2. Barteau et al. also summarize several mechanisms involving the intermediate of acid anhydride [9]. In addition to the mechanisms, the reasons of high catalytic activity of oxides for ketonization have been proposed: the high catalytic activity relates to crystal structure [7,27], bond strength between metal and oxygen [3], and presence of Lewis acid and base sites [28].

Although silica-supported La_2O_3 and Nd_2O_3 have been previously reported as catalysts which show high catalytic activity for the ketonization of carboxylic acid [13], no systematic study has been conducted to explain the ketonization. Therefore, in this work, we investigated a series of rare earth oxides (REOs) as catalysts for the ketonization of acetic acid. The REOs were calcined at 1000 °C to clarify the relation between the crystal structure and the catalytic activity of REOs. We confirmed that especially four REOs such as La_2O_3, CeO_2, Pr_6O_{11}, and Nd_2O_3 among the tested REOs catalyzed the ketonization of acetic acid to produce acetone, and characterized the active REOs. We also proposed probable mechanisms of ketonization over REOs and discussed the reason for the high catalytic activity of the active REOs.

2. Experimental

2.1. Samples

Acetic acid was purchased from Wako Pure Chemical Industries, Ltd., Japan, and was used for the catalytic reaction without further purification. All of REOs such as La_2O_3, CeO_2, Pr_6O_{11}, Nd_2O_3, Sm_2O_3, Eu_2O_3, Gd_2O_3, Tb_4O_7, Dy_2O_3, Ho_2O_3, Er_2O_3, Tm_2O_3, Yb_2O_3, and Lu_2O_3 were purchased from Kanto Chemical Co., Inc. All of the oxides were calcined at 1000 °C prior to reaction. The particle size of REO used in this study was in the range from 125 to 850 μm.

* Corresponding authors. Tel.: +81 43 290 3376; fax: +81 43 290 3401.
E-mail addresses: y-yamada@faculty.chiba-u.jp (Y. Yamada), satoshi@faculty.chiba-u.jp (S. Sato).

1381-1169/$ – see front matter © 2011 Elsevier B.V. All rights reserved.
doi:10.1016/j.molcata.2011.06.011

2.2. Catalytic reaction

Each reaction was carried out in a conventional fixed-bed down flow glass tube reactor with an inner diameter of 17 mm at 350 °C under the atmospheric pressure of N_2. REOs (weight, 0.5 g) were supported on a glass wool in the reactor, and the temperature of the REO bed (height, ca. 5 mm) was monitored with a thermocouple located in the REO bed. Prior to the reaction of acetic acid, REOs were heated in the reactor in N_2 flow at 500 °C for 1 h. After the catalyst had been cooled to 350 °C, acetic acid was fed through the top of the reactor at liquid feed rate of 2.67 $cm^3\ h^{-1}$ (46.6 mmol h^{-1}) together with N_2 flow of 30 $cm^3\ min^{-1}$. An effluent was collected every 30 min, and analyzed by GC–MS (Shimadzu GCMS-QP5050) and FID-GC (Shimadzu GC-8A) using a 30-m capillary column of Inertcap-WAX (GL Science).

2.3. Characterization of catalysts

The specific surface areas of catalysts, SA, were calculated with the BET method using N_2 isotherm at −196 °C. X-ray diffraction (XRD) patterns were recorded on an M18XHF (Mac Science, Japan) using CuKα radiation (λ = 0.15 nm) to determine crystal structure of REOs. Thermogravimetry–differential thermal analysis (TG–DTA) was conducted in air using Thermo plus TG8120 (Rigaku Corp., Japan). Structural feature of the REOs was characterized by diffuse reflectance infrared Fourier transform (DRIFT) spectrometer with a mercury cadmium telluride detector (JASCO Corp., Japan).

3. Results

3.1. Catalytic reactions of acetic acid over REOs

We have already reported changes in the structures of the as-received REOs by being calcined at 1000 °C [29,30]. Fig. 1 summarizes the XRD patterns of REOs calcined at 1000 °C while some XRD data are cited from Refs. [29,30]. Crystal structures of the as-received La_2O_3 and Nd_2O_3 are hexagonal, and those of as-received Sm_2O_3, Eu_2O_3, Gd_2O_3, Dy_2O_3, Ho_2O_3, Er_2O_3, Tm_2O_3, Yb_2O_3, and Lu_2O_3 are monoclinic, while CeO_2 is fluorite. Pr_6O_{11} is composed of two structures such as hexagonal and fluorite, and Tb_4O_7 is composed of monoclinic and fluorite [31]. Due to the crystal growth of La_2O_3 and Nd_2O_3 upon calcinations, intensity of the pattern is increased. Sm_2O_3, Eu_2O_3, and Gd_2O_3 keep their monoclinic structure even after being calcined at 1000 °C. Crystal structures of Dy_2O_3, Ho_2O_3, Er_2O_3, Tm_2O_3, Yb_2O_3, and Lu_2O_3 are transformed into bixbyite of cubic structure by being calcined at 1000 °C. CeO_2 keeps its original fluorite structure even after calcinations. Crystal structures of Pr_6O_{11} and Tb_4O_7 are transformed into fluorite structure [29].

Table 1 shows the catalytic activity of REOs calcined at 1000 °C. Among REOs we tested, four REOs such as La_2O_3, CeO_2, Pr_6O_{11}, and Nd_2O_3 showed high catalytic activity at 350 °C. Especially, Pr_6O_{11} showed the highest yield of 80% among all of the tested REOs. Other 10 REOs were not so active while the selectivity to acetone decreased with increasing the atomic number of rare earth metal in REOs. Over the less active REOs, a by-product of this reaction was mainly acetic anhydride. Fig. 2 shows the dependency of the catalytic activity on the time on stream at 350 °C. Light REOs such as La_2O_3 showed stable catalytic activity at least for 2.5 h: conversion exceeds 77%. On the other hand, heavy REOs such as Yb_2O_3 lost the catalytic activity drastically within 1 h: the amount of produced acetone decreased with time on stream. This tendency seems to be related to the decomposition temperature of the corresponding rare earth acetate, which will be discussed later.

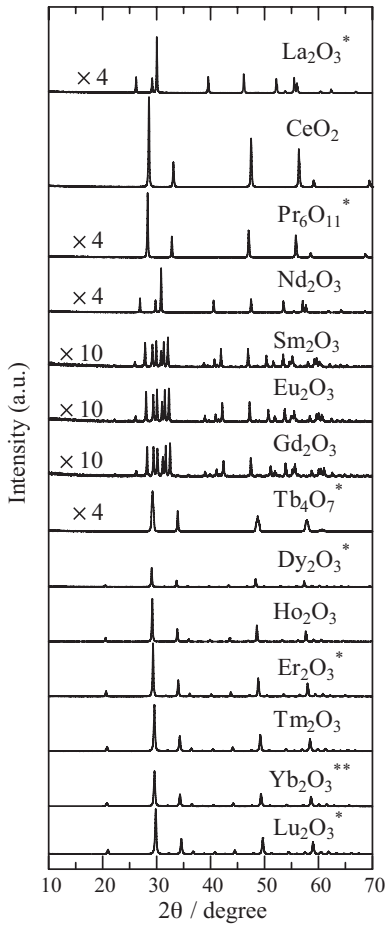

Fig. 1. XRD profiles of REOs calcined at 1000 °C. *Data referred from Ref. [29]. **Data cited from Ref. [30].

Judging from the results in Table 1 and Fig. 1, it is clear that the catalytic activity of REOs has little dependence on the crystal structure for the ketonization reaction. Since the crystal structure has little influence on the catalytic activity, other factors are expected to affect the catalytic activity of REOs. Therefore, the composition

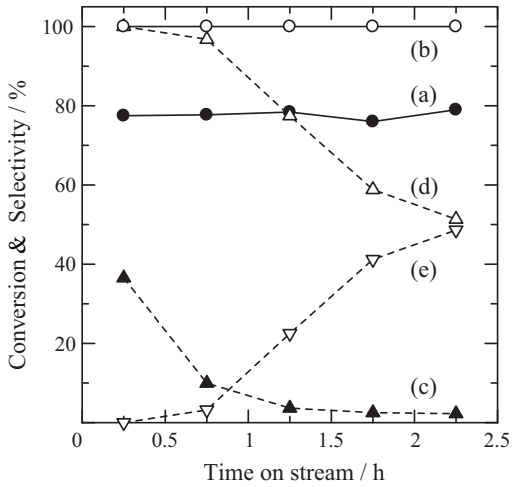

Fig. 2. Time course of ketonization of acetic acid over La_2O_3 and Yb_2O_3 at 350 °C. (a) Conversion and (b) selectivity to acetone over La_2O_3. (c) Conversion and (d) selectivity to acetone and (e) to acetic anhydride over Yb_2O_3. W/F = 0.187 g h cm^{-3} where W and F are catalyst weight and flow rate reactant fed, respectively. W = 0.5 g and F = 2.67 $cm^3\ h^{-1}$. N_2 carrier gas flow rate is 30 $cm^3\ min^{-1}$.

Table 1
Conversion and selectivity of acetic acid at 350 °C over REOs calcined at 1000 °C.

Oxides	SA ($m^2\ g^{-1}$)	Conv. (%)	Selectivity (mol%)			Acetone yield (%)
			Acetone	Ac_2O	Others[a]	
La_2O_3	6.8	77.7	99.9	0.0	0.1	77.6
CeO_2	13.2	51.3	99.9	0.0	0.1	51.2
Pr_6O_{11}	4.6	80.1	99.9	0.0	0.1	80.0
Nd_2O_3	3.7	37.9	100.0	0.0	0.0	37.9
Sm_2O_3	6.4	10.2	96.3	3.7	0.0	9.8
Eu_2O_3	16.4	13.6	95.1	4.8	0.1	12.9
Gd_2O_3	7.3	7.3	94.5	5.5	0.0	6.9
Tb_4O_7	9.3	7.6	94.3	4.8	0.9	7.2
Dy_2O_3	11.1	6.4	86.1	13.9	0.0	5.5
Ho_2O_3	11.2	4.3	81.2	18.8	0.0	3.5
Er_2O_3	13.6	9.6	78.0	22.0	0.0	7.5
Tm_2O_3	16.1	3.8	65.9	30.4	3.7	2.5
Yb_2O_3	15.7	11.0	76.9	23.1	0.0	8.5
Lu_2O_3	14.1	14.6	75.9	22.7	1.4	11.1

Conversion and selectivity were averaged in the initial 2.5 h. $W/F = 0.187\ g\ h\ cm^{-3}$ where W and F are catalyst weight and flow rate reactant fed, respectively. $W = 0.5$ g and $F = 2.67\ cm^3\ h^{-1}$. N_2 carrier gas flow rate is $30\ cm^3\ min^{-1}$. Ac_2O is acetic anhydride.
[a] Others contain 4-methyl-3-penten-2-one, 4-methyl-4-penten-2-one, trimethylbenzene, and 2-cyclohexen-1-one.

Table 2
Temperature dependence on the ketonization of acetic acid over La_2O_3 calcined at 1000 °C.

Reaction temperature (°C)	Conv. (%)	Selectivity (mol%)			Acetone yield (%)
		Acetone	Ac_2O	Others[a]	
325	6.0	97.9	2.1	0.0	5.9
350	77.7	99.9	0.0	0.1	77.6
375	59.1	99.9	0.0	0.1	59.0
400	65.2	99.9	0.0	0.1	65.1
425	68.1	99.6	0.0	0.4	67.8

Reaction conditions and footnote "a" are the same as those in Table 1.

and functional groups of reacted REOs with acetic acid were investigated using XRD, TG–DTA, and DRIFT in the following section.

Table 2 shows the temperature dependence on the catalytic activity of La_2O_3 calcined at 1000 °C. At the reaction temperature of 325 °C, the conversion of acetic acid was as low as 6%. The conversion drastically increased from 325 °C to 350 °C, and it showed a maximum at 350 °C. The conversion gradually increased with increasing the reaction temperature from 375 to 425 °C.

3.2. Characterization of active REOs in the ketonization

Fig. 3 shows the XRD patterns of La_2O_3, CeO_2, Pr_6O_{11}, and Nd_2O_3 after reacting with acetic acid at 350 °C. La_2O_3 was converted into another compound after being reacted with acetic acid, as observed in Fig. 3b. Among four active REOs, Pr_6O_{11} and Nd_2O_3 showed a similar tendency to La_2O_3 in the structural changes after being reacted with acetic acid at 350 °C (Fig. 3d and e, respectively). We did not find the diffraction patterns in the ICDD cards, while we can identify the compound observed in Fig. 3d as PrO(AcO), where AcO indicates CH_3COO group, by comparing XRD profile of PrO(AcO) reported in Ref. [32]. LaO(AcO) and NdO(AcO) would be also produced after acetic acid contacted La_2O_3 and Nd_2O_3, respectively. In contrast, only CeO_2 among the active REOs showed no significant structural change after ketonization: CeO_2 remained its fluorite structure even after being reacted with acetic acid, as determined by XRD (Fig. 3c).

Fig. 4a shows a TG–DTA profile of La_2O_3 reacted with acetic acid at 350 °C for 2.5 h. The sample shows severe weight loss between 300 °C and 440 °C together with the exothermic peaks at 320 °C and 430 °C. The weight loss and exothermic peaks indicate that La_2O_3 was converted into another compound containing organic species during ketonization. Since the structure of La_2O_3 was converted into an organic compound by being reacted

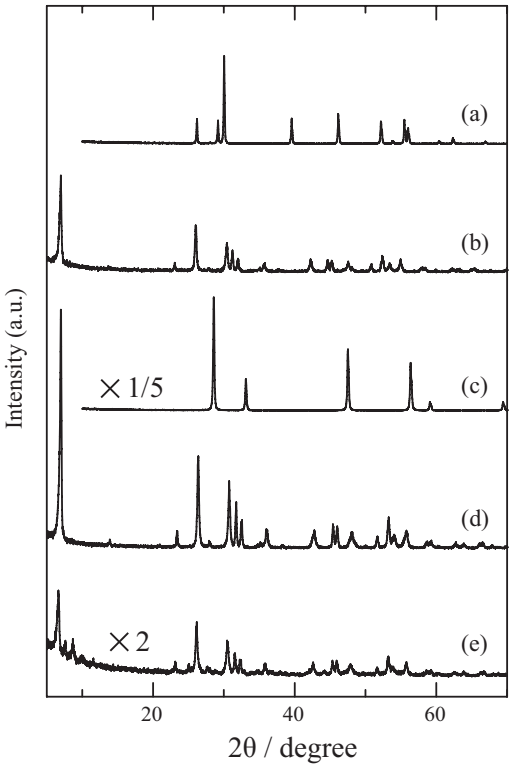

Fig. 3. XRD pattern of REOs after reaction with acetic acid at 350 °C. (a) Fresh La_2O_3 calcined at 1000 °C, (b) La_2O_3 after reaction, (c) CeO_2 after reaction, (d) Pr_6O_{11} after reaction, and (e) Nd_2O_3 after reaction.

with acetic acid, decomposition process of $La(AcO)_3{\cdot}H_2O$ was analyzed for the discussion on the active species in the ketonization. Fig. 4b shows a TG–DTA profile of $La(AcO)_3{\cdot}H_2O$. Three exothermic peaks were observed at 328, 342, and 394 °C in the profile.

Fig. 5 shows the DRIFT spectra of La_2O_3 and CeO_2 reacted with acetic acid at 350 °C. In Fig. 5a, La_2O_3 reacted with acetic acid showed peaks at around 922, 1010, and 1054 cm^{-1} which originates from acetate, whereas they were not observed in La_2O_3 (spectrum is not shown). Peaks at around 3000 cm^{-1} are stretching vibration of C–H in CH_3 group of acetate [28,33–35]. In Fig. 5b, as a result of DRIFT analysis, acetate species seem to be present on the surface of CeO_2 reacted with acetic acid at 350 °C: C–H stretching vibration at 2941 cm^{-1} and C=O stretching vibration at 1690 cm^{-1} were observed. In addition, we also observed DRIFT spectra on Pr_6O_{11} and Nd_2O_3 reacted with acetic acid at 350 °C similar to the spectrum in Fig. 5a (spectra are not shown).

3.3. Transformation of La_2O_3 into LaO(AcO) during induction period of the ketonization

Induction period was observed in the initial period after acetic acid was fed through the reactor top: no organic species was collected in the initial reaction period for several minutes. In order to evaluate the conversion rate of La_2O_3 to acetate species, after acetic acid had been contacted with La_2O_3 at the feed rate of

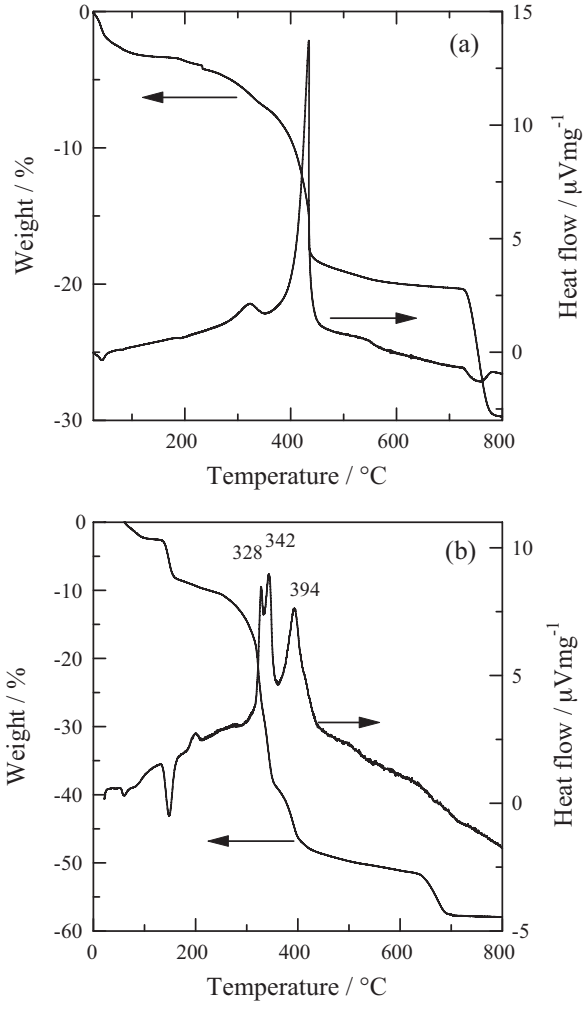

Fig. 4. TG–DTA profiles of (a) La_2O_3 reacted with acetic acid at 350 °C for 2.5 h and (b) $La(AcO)_3{\cdot}H_2O$ reagent. The TG–DTA was performed in air.

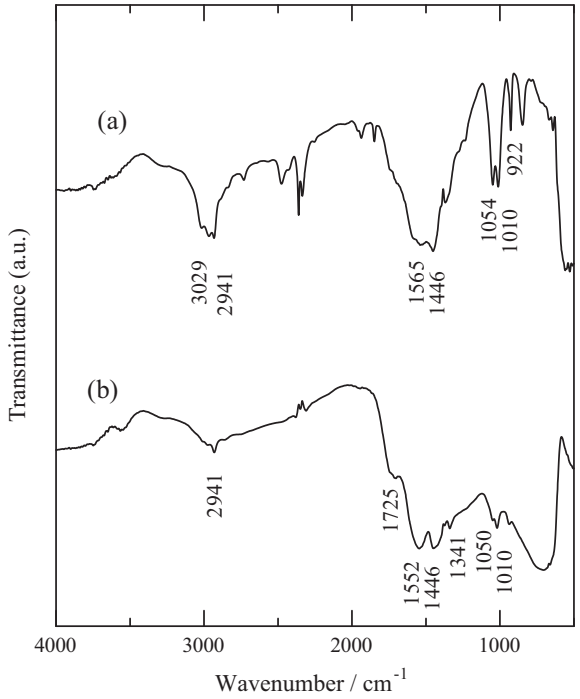

Fig. 5. DRIFT spectra of REOs after reaction with acetic acid at 350 °C. (a) La_2O_3, (b) CeO_2.

0.78 mmol min^{-1} and 350 °C, an effluent collected in each trap was analyzed by FID-GC. Fig. 6 plots the detected amounts of produced acetone and unreacted acetic acid against the amounts of fed acetic acid. The molar quantity of La_2O_3 (0.5 g) used in this experiment is ca. 1.5 mmol, which corresponds to 3.1 mmol of atomic La. The total molar quantity of acetone produced by feeding 7.7 mmol of acetic acid is 1.4 mmol. This indicates that ca. 4.9 (=7.7 − 2 × 1.4) mmol of acetic acid was missing in the duration. Acetic acid had not been recovered until 7.7 mmol of acetic acid was fed, while unreacted acetic acid started being detected after 11.6 mmol was fed. After

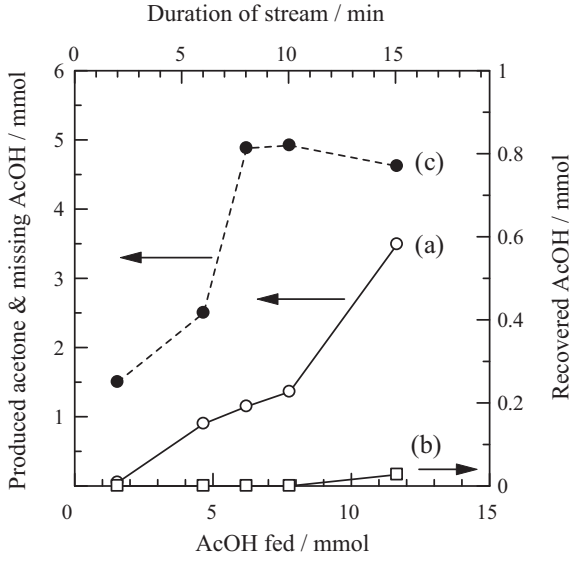

Fig. 6. Amounts of acetone produced over La_2O_3 in the initial periods of reaction with acetic acid at 350 °C. The produced acetone (a) and recovered acetic acid (b) in the effluent were determined by GC-FID, and missing acetic acid (c) was calculated. An effluent was collected in the trap during each plot over 0.5 g of La_2O_3 including 3.1 mmol of atomic La.

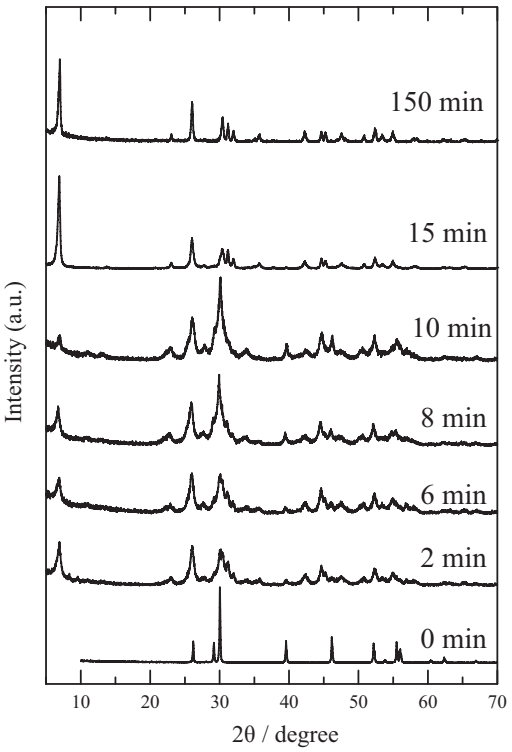

Fig. 7. Changes in the XRD profile of La_2O_3 after reacting with acetic acid at 350 °C with time on stream. Numbers in the figure indicate the duration of stream, which is the same as that in Fig. 6.

11.6 mmol of acetic acid was fed, unreacted acetic acid was recovered, and the amount of produced acetone was more than twice that of acetone produced before 7.7 mmol of acetic acid was fed. It means that acetic acid was totally consumed and converted into acetone. Therefore, it is estimated that 1.58 mol of acetic acid per 1 mol of La disappears in the initial period of reaction.

Fig. 7 shows structural changes in La_2O_3 catalysts during the initial period of ketonization at 350 °C. In the initial periods for 10 min in Fig. 7, La_2O_3 samples that contacted with 1.5–7.7 mmol of acetic acid consisted of imperfect LaO(AcO) structure. The imperfect LaO(AcO) was obtained until 11.6 mmol was fed probably due to the thickness of the loaded catalyst bed. Perfect LaO(AcO) was observed at the fed amount of 11.6 mmol (Fig. 7, 15 min). More than 8 mmol of acetic acid was necessary to convert all of 1.5 mmol of La_2O_3 into LaO(AcO). These phenomena notify us that the formation of LaO(AcO) is completed in the initial period of the reaction together with the formation of acetone, and the ketonization steadily proceeds through the catalytic cycle together with the conversion between LaO(AcO) and $La_2O(AcO)_4$ after the initial period.

4. Discussion

4.1. Catalytic activity of REOs for ketonization of acetic acid

In Table 1, the conversion and selectivity tend to become high, as the atomic number of REOs decreases. Since the strength of basicity of light REOs is higher than that of heavy REOs [29], the high catalytic activity for ketonization reaction could be basically due to the presence of strong basic site, whereas CeO_2 is an exception. The by-product of this reaction over heavy REOs was mainly acetic anhydride. It is reported that condensation of acetic acid into acetic anhydride occurs at temperature higher than 700 °C but an aid of acid catalysts lowers the reaction temperature [36]. In this work, acetic anhydride is considered to be formed due to the low basicity of heavy REOs.

Heavy REOs, such as Ho_2O_3 and Er_2O_3, show low catalytic activity for ketonization (Table 1). In the initial period of ketonization over La_2O_3 (Fig. 6), it is suggested that La_2O_3 is converted to one kind of lanthanum acetate (Fig. 3b). In order to ensure the decomposition behavior of the acetate, Schemes 1 and 2 cited the decomposition steps of $Ce(AcO)_3{\cdot}H_2O$ [37] and $Ho(AcO)_3{\cdot}3.5H_2O$ [38] in TG–DTA profiles, respectively. According to Scheme 1 [37], in the decomposition of $Ce(AcO)_3$ at around 300 °C, cerium(III) acetate such as $Ce(AcO)_3$ is decomposed into oxyacetate such as $Ce_2O(AcO)_4$ and CeO(AcO) to produce acetone and CO_2. In the last step, CeO(AcO) is decomposed into $Ce_2O_2CO_3$ to produce acetone at 355 °C. In contrast to the presence of $Ce_2O(AcO)_4$, $Ho_2O(AcO)_4$ is not present during the decomposition of $Ho(AcO)_3$ in Scheme 2 [38]. $Ho(AcO)_3$ is decomposed into oxyacetate such as HoO(AcO) to produce acetic acid at 280 and 330 °C. Similar to the decomposition

$2\ Ce(AcO)_3{\cdot}H_2O \rightarrow 2\ Ce(AcO)_3 + H_2O$	(130 °C)	I
$2\ Ce(AcO)_3 \rightarrow Ce_2O(AcO)_4 + CH_3COCH_3 + CO_2$	(287 °C)	II
$Ce_2O(AcO)_4 \rightarrow 2\ CeO(AcO) + CH_3COCH_3 + CO_2$	(307 °C)	III
$2\ CeO(AcO) \rightarrow Ce_2O_2CO_3 + CH_3COCH_3$	(355 °C)	IV
$Ce_2O_2CO_3 \rightarrow CeO_2 + CO$	(800 °C)	V
$2\ Ce(AcO)_3{\cdot}H_2O \rightarrow CeO_2 + 3\ CH_3COCH_3 + 2\ CO_2 + CO + H_2O$		

Scheme 1. Thermal decomposition of $Ce(AcO)_3{\cdot}H_2O$ in air [37].

$2\ Ho(AcO)_3{\cdot}3.5H_2O \rightarrow 2\ Ho(AcO)_3 + 3.5\ H_2O$	(105 °C)	I
$2\ Ho(AcO)_3 \rightarrow 2\ Ho(OH)(AcO)_2 + 2\ H_2C\text{-}C{=}O$	(280 °C)	II-1
$2\ H_2C\text{-}C{=}O + 2\ H_2O \rightarrow 2\ AcOH$		II-2
$2\ Ho(OH)(AcO)_2 \rightarrow 2\ HoO(AcO) + 2\ AcOH$	(330 °C)	III
$2\ HoO(AcO) \rightarrow Ho_2O_2CO_3 + CH_3COCH_3$	(390 °C)	IV
$Ho_2O_2CO_3 \rightarrow Ho_2O_3 + CO_2$	(590 °C)	V
$2\ Ho(AcO)_3{\cdot}3.5H_2O \rightarrow Ho_2O_2CO_3 + CH_3COCH_3 + 4\ AcOH + CO_2$		

Scheme 2. Thermal decomposition of $Ho(AcO)_3{\cdot}3.5H_2O$ in air [38].

$2\ La(AcO)_3{\cdot}nH_2O \rightarrow 2\ La(AcO)_3 + nH_2O$	(147 °C)	I
$2\ La(AcO)_3 \rightarrow La_2O(AcO)_4 + CH_3COCH_3 + CO_2$	(328 °C)	II
$La_2O(AcO)_4 \rightarrow 2\ LaO(AcO) + CH_3COCH_3 + CO_2$	(342 °C)	III
$2\ LaO(AcO) \rightarrow La_2O_2CO_3 + CH_3COCH_3$	(394 °C)	IV
$La_2O_2CO_3 \rightarrow La_2O_3 + CO_2$	(669 °C)	V
$2\ La(AcO){\cdot}nH_2O \rightarrow La_2O_3 + 3\ CH_3COCH_3 + 3\ CO_2 + nH_2O$		

Scheme 3. Thermal decomposition of $La(AcO)_3{\cdot}nH_2O$ in air determined by TG–DTA, XRD, and DRIFT measurement in this work.

of CeO(AcO), HoO(AcO) is decomposed into $Ho_2O_2CO_3$ to produce acetone at 390 °C. In this way, the ketone is probably formed by the decomposition of acetate and oxyacetates. In addition, decomposition of $Pr(AcO)_3$ [32] and $Nd(AcO)_3$ [39] has already been reported elsewhere.

Among the four active REOs, only CeO_2 shows no structural change after ketonization (Fig. 3c): CeO_2 retains its fluorite structure even after being reacted with acetic acid at 350 °C. However, adsorbed acetate species was observed on the surface of CeO_2 (Fig. 5b). It is reasonable that the adsorbed acetate is an intermediate species in the ketonization of acetic acid. Namely, surface reaction of ketonization such as Schemes 1–3 is possible in the catalytic formation of acetone from acetic acid. To accomplish the catalytic cycle of ketonization, the surface of CeO_2 has to store more acetate species in the atmosphere of acetic acid vapor. Therefore, it can be explained that the formation of surface acetate proceeds only on the surface of CeO_2 during the reaction of acetic acid over CeO_2. In any case, the surfaces of four active REOs are converted into MO(AcO), where M is La, Ce, Pr, and Nd. Therefore, the formation of MO(AcO) would be one of the important factors for ketonization of acetic acid.

In Fig. 4a, the weight loss at around 400 °C and 750 °C can be regarded as the release of acetone and CO_2, respectively. The total weight loss by ca. 23% from 350 to 800 °C is consistent with those of acetone (molecular weight, MW = 58.0) and CO_2 (MW = 44.0) removed from a sample composed of LaO(AcO) (formula weight = 213.9). In Fig. 4b, we analyzed the decomposition process of reagent $La(AcO)_3{\cdot}H_2O$ during the TG–DTA in air. The weight loss in the TG is considered to be due to H_2O, acetone and CO_2. Each decomposition step, which was estimated from the weight loss of Fig. 4, is summarized in Scheme 3. $La(AcO)_3{\cdot}H_2O$ would be converted into La_2O_3 with five steps that resemble the decomposition of $Ce(AcO)_3{\cdot}H_2O$ in Scheme 1 [37]. In the TG–DTA profile of La_2O_3 reacted with acetic acid at 350 °C for 2.5 h (Fig. 4a), an exothermic peak at 320 °C is probably due to the decomposition of $La_2O(AcO)_4$ into LaO(AcO). The main exothermic peak at ca. 400 °C is monitored due to the decomposition of LaO(AcO) to oxycarbonate, $La_2O_2(CO_3)$, as expressed in Schemes 3–5.

TG–DTA of the catalysts was conducted in air whereas all catalytic measurements were carried out in a stream of N_2. It is known that the composition of a gaseous atmosphere during the thermal decomposition of a substance can influence the route of the decomposition and its rate. The difference in atmosphere has been investigated on $Pr(AcO)_3$ [32]: no significant difference between in air and in N_2 was found on the TG profiles below 600 °C. Therefore, we can discuss mechanisms of the catalytic cycle under these conditions without caution.

4.2. Probable reaction mechanism over REOs

Judging from the results in Figs. 6 and 7, we propose a probable catalytic cycle of the ketonization of acetic acid over La_2O_3 in Scheme 4. Acetic acid is converted into acetone at the acetic acid/acetone ratio of 4 in the initial period of the reaction with acetic acid (Scheme 4a), and the ratio changes into 2 in the steady state of the reaction (Scheme 4b). Since a similar tendency was observed for Pr_2O_3 and Nd_2O_3, the reaction drawn in Scheme 4 is also applied to Pr_2O_3 and Nd_2O_3.

Here, we propose that MO(AcO), M = La, Pr, and Nd, is probably the active catalyst species. $M_2O(AcO)_4$ is formed by contacting acetic acid with oxides, and then $M_2O(AcO)_4$ decomposes into MO(AcO) as well as acetone is formed (Scheme 4a). Once M_2O_3 was converted into MO(AcO) completely, the ketonization proceeds catalytically via a catalytic cycle such as Scheme 4b. In this scheme, MO(AcO) is the active catalyst species and $M_2O(AcO)_4$ is an intermediate. In the comparison of REOs for the ketonization of acetic acid, we can propose more precise reaction path than the previous reports [13,28].

In Scheme 5, we propose the most probable reaction mechanism for the ketonization of acetic acid over REOs. At the first step,

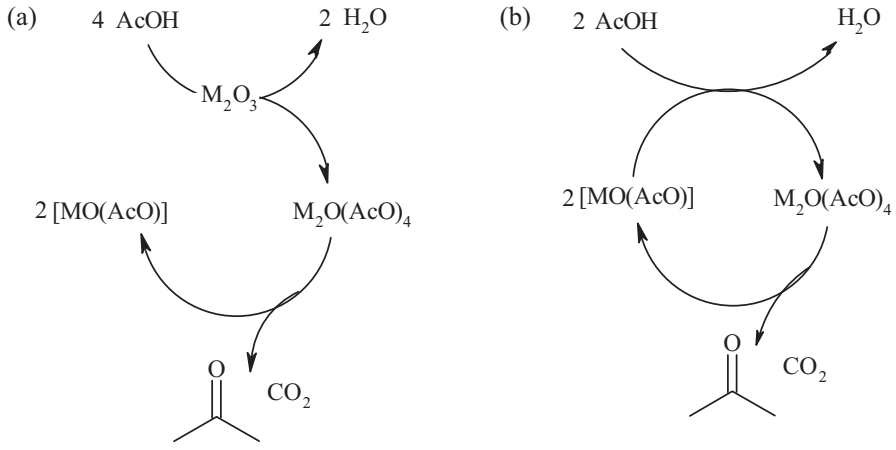

Scheme 4. Proposed catalytic cycle for ketonization of acetic acid over REOs. (a) Initiation reaction in which oxides were converted into oxyacetates. (b) Catalytic cycle after M_2O_3 was totally converted into MO(AcO). M = La, Pr, and Nd.

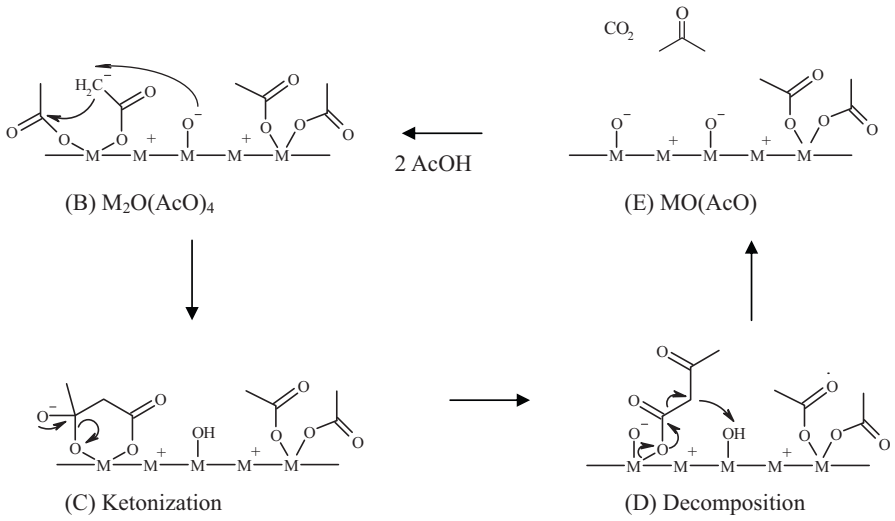

Scheme 5. Speculative reaction mechanism for ketonization of acetic acid over M_2O_3 where M = La, Pr, and Nd.

M_2O_3 is converted into $M_2O(AcO)_4$, α-hydrogen on acetate is subtracted by the basic oxygen on oxide to produce carbanion. Then, the produced carbanion attacks the carbon of neighboring C=O nucleophilically, and β-ketoacetate is formed via the condensation reaction. Finally, the β-ketoacetate decomposes into CO_2 and acetone, and the structure of the catalyst becomes $M_2O_2(AcO)_2$ that is equal to MO(AcO). This route is essentially the same as a previously proposed mechanism [24].

Low catalytic activity of REOs such as Ho_2O_3 is also explainable from Scheme 5. It is speculated that the catalytic cycle of HoO(AcO) and $Ho_2O(AcO)_4$ does not proceed in the reaction of acetic acid over Ho_2O_3. As discussed in Section 4.1, $Ho_2O(AcO)_4$ is not formed in the decomposition process of $Ho(AcO)_3$. In addition, the catalytic activity of Sm_2O_3 is also low, as demonstrated in Table 1. This is explained by the thermal decomposition temperature of $Sm(AcO)_3$, 390 °C, which is higher than the reaction temperature of 350 °C [40].

4.3. Dependence of catalytic activity on specific surface area of REOs

Fig. 8 plots the yield of acetone versus specific surface area of the recovered REO catalysts, which are LaO(AcO), CeO_2, PrO(AcO), and NdO(AcO). Extrapolation of the linear line converges near zero surface area: the yield of acetone is proportional to the specific surface area of the catalyst. Therefore, ketonization over REOs proceeds on the surface of catalyst samples and there is no relevancy with crystal structure or planes, although there are some reports that the activity of oxides depends on their crystal planes [7,14,27]. For example, the crystal structure of CeO_2, Pr_6O_{11}, and Tb_4O_7 calcined at 1000 °C is cubic fluorite (Fig. 1), but the conversion of acetic acid is low only over Tb_4O_7. In a similar manner, bixbyite of heavy REOs, such as Dy_2O_3, Yb_2O_3 and Lu_2O_3, and fluorite CeO_2 have close cubic structure (Fig. 1), but the conversion of acetic acid is high only over CeO_2. It can be summarized that crystal structures of REOs are independent of the catalytic activity of REOs.

In Table 2, the conversion over La_2O_3 at 350 °C is higher than that at 375 °C, and the conversion gradually increased with increasing the reaction temperature from 375 to 425 °C. This temperature dependence can be explained by the formation of LaO(AcO) into $La_2O_2CO_3$ (Fig. 4a and Schemes 3–5): the surface of $La_2O_2CO_3$ is less active than that of LaO(AcO). It can be explained that the conversion over $La_2O_2CO_3$ could be increased with an increase in temperature

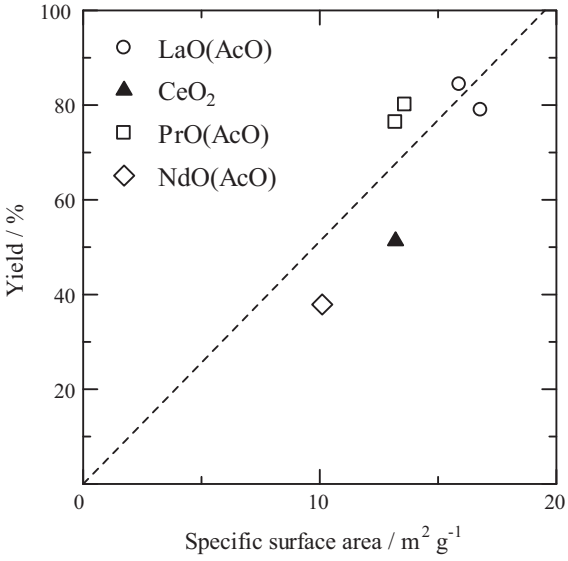

Fig. 8. Yield of acetone at 350 °C versus specific surface area of catalysts after ketonization.

from 375 to 425 °C. We need further research on the ketonization at different temperatures.

5. Conclusions

A series of REOs were investigated for ketonization of acetic acid at 350 °C: the acetic acid conversion of 38–80% and the selectivity to acetone over 99.9% were obtained over REOs such as La_2O_3, CeO_2, Pr_6O_{11}, and Nd_2O_3. Especially, Pr_6O_{11} showed the highest yield of 80% and Nd_2O_3 showed the highest selectivity of 100% among fourteen REOs. Four active REO catalysts converted into an oxyacetate such as MO(AcO), M = La, Pr, and Nd, after ketonization. On the other hand, the bulk structure of CeO_2 is retained during the ketonization while the surface of CeO_2 is converted into acetate. The yield of acetone was proportional to the specific surface area of the produced oxyacetate and CeO_2, and the linear extrapolation goes through near the origin. It is concluded that the ketonization of acetic acid over REOs proceeds on the surface of the oxyacetate such as MO(AcO) via the catalytic cycle between MO(AcO)

and $M_2O(AcO)_4$ to produce acetone and CO_2 with the consumption of acetic acid.

References

[1] M. Gliński, W. Szymański, D. Lomot, Appl. Catal. A 281 (2005) 107–113.
[2] R. Pestman, R.M. Koster, J.A.Z. Pieterse, V. Ponec, J. Catal. 168 (1997) 255–264.
[3] R. Pestman, R.M. Koster, A. van Duijne, J.A.Z. Pieterse, V. Ponec, J. Catal. 168 (1997) 265–272.
[4] J.C. Kuriacose, R. Swaminathan, J. Catal. 14 (1969) 348–354.
[5] R. Swaminathan, J.C. Kuriacose, J. Catal. 16 (1970) 357–362.
[6] M. Jayamani, C.N. Pillai, J. Catal. 87 (1984) 93–97.
[7] K.S. Kim, M.A. Barteau, J. Catal. 125 (1990) 353–375.
[8] R. Pestman, A. van Duijne, J.A. Pieterse, V. Ponec, J. Mol. Catal. A: Chem. 103 (1995) 175–180.
[9] R. Martinez, M.C. Huff, M.A. Barteau, J. Catal. 222 (2004) 404–409.
[10] K. Okumura, Y. Iwasawa, J. Catal. 164 (1996) 440–448.
[11] K. Parida, H.K. Mishra, J. Mol. Catal. A 139 (1999) 73–80.
[12] M. Gliński, J. Kijeński, Appl. Catal. A 190 (2000) 87–91.
[13] M. Gliński, J. Kijeński, A. Jakubowski, Appl. Catal. A: Gen. 128 (1995) 209–217.
[14] J. Stubenrauch, E. Brosha, J.M. Vohs, Catal. Today 28 (1996) 431–441.
[15] M. Gliński, J. Kijeński, React. Kinet. Catal. Lett. 69 (2000) 123–128.
[16] S.D. Randery, J.S. Warren, K.M. Dooley, Appl. Catal. A 226 (2002) 265–280.
[17] T.S. Hendren, K.M. Dooley, Catal. Today 85 (2003) 333–351.
[18] E.J. Grootendorst, R. Pestman, R.M. Koster, V. Ponec, J. Catal. 148 (1994) 261–269.
[19] R. Pestman, R.M. Koster, E. Boellaard, A.M. van der Kraan, V. Ponec, J. Catal. 174 (1998) 142–152.
[20] Y. Wang, B.H. Davis, Appl. Catal. A 180 (1999) 277–285.
[21] K.M. Parida, A. Samal, N.N. Das, Appl. Catal. A 166 (1998) 201–205.
[22] S. Sugiyama, K. Sato, S. Yamasaki, K. Kawashiro, H. Hayashi, Catal. Lett. 14 (1992) 127–133.
[23] K. Parida, J. Das, J. Mol. Catal. A 151 (2000) 185–192.
[24] O. Nagashima, S. Sato, R. Takahashi, T. Sodesawa, J. Mol. Catal. A: Chem. 227 (2005) 231–239.
[25] C.A. Gaertner, J.C. Serrano-Ruiz, D.J. Braden, J.A. Dumesic, J. Catal. 266 (2009) 71–78.
[26] M. Renz, Eur. J. Org. Chem. 2005 (2005) 979–988.
[27] M.A. Barteau, J. Vac. Sci. Technol. A 11 (1993) 2162–2168.
[28] M.A. Hasan, M.I. Zaki, L. Pasupulety, Appl. Catal. A: Gen. 243 (2003) 81–92.
[29] S. Sato, R. Takahashi, M. Kobune, H. Gotoh, Appl. Catal. A: Gen. 356 (2009) 57–63.
[30] A. Igarashi, S. Sato, R. Takahashi, T. Sodesawa, M. Kobune, Catal. Commun. 8 (2007) 807–810.
[31] M. Zinkevich, Prog. Mater. Sci. 52 (2007) 597–647.
[32] B.M. Abu-Zied, S.A. Soliman, Thermochim. Acta 470 (2008) 91–97.
[33] S. Valange, A. Beauchaud, J. Barrault, Z. Gabelica, M. Daturi, F. Can, J. Catal. 251 (2007) 113–122.
[34] G.A.H. Mekhemer, S.A. Halawy, M.A. Mohamed, M.I. Zaki, J. Catal. 230 (2005) 109–122.
[35] Z.F. Pei, V. Ponec, Appl. Surf. Sci. 103 (1996) 171–182.
[36] N.Y. He, C.S. Woo, H.G. Kim, H.I. Lee, Appl. Catal. A: Gen. 281 (2005) 167–178.
[37] T. Arii, T. Taguchi, A. Kishi, M. Ogawa, Y. Sawada, J. Eur. Ceram. Soc. 22 (2002) 2283–2289.
[38] G.A.M. Hussein, B.A.A. Balboul, G.A.H. Mekhemer, J. Anal. Appl. Pyrol. 56 (2000) 263–272.
[39] L. Kepinski, M. Zawadzki, W. Mišta, Solid State Sci. 6 (2004) 1327–1336.
[40] R.M. Mahfouz, M.A.S. Monshi, S.M. Alshehri, N.M. Abd El-Salam, Radiat. Phys. Chem 59 (2000) 381–385.